Published in final edited form as:
J Neural Eng. 2006 June ; 3(2): 79–86. doi:10.1088/1741-2560/3/2/001.

Photometric recording of transmembrane potential in outer hair cells

Takashi Nakagawa[1,4], **John S Oghalai**[1], **Peter Saggau**[2], **Richard D Rabbitt**[3], and **William E Brownell**[1,2]

[1] Bobby R Alford Department of Otolaryngology—Head and Neck Surgery, Baylor College of Medicine, Houston, TX 77030, USA

[2] Department of Neuroscience, Baylor College of Medicine, Houston, TX 77030, USA

[3] Departments of Bioengineering and Surgery, University of Utah, Salt Lake City, UT 84112, USA

Abstract

Cochlear outer hair cells (OHCs) are polarized epithelial cells that have mechanoelectrical transduction channels within their apical stereocilia and produce electromotile force along their lateral wall. Phase shifts, or time delays, in the transmembrane voltage occurring at different axial locations along the cell may contribute to our understanding of how these cells operate at auditory frequencies. We developed a method to optically measure the phase of the OHC transmembrane potential using the voltage-sensitive dye (VSD) di-8-ANEPPS. The exit aperture of a fibre-optic light source was driven in two dimensions so that a 24 μm spot of excitation light could be positioned along the length of the OHC. We used the whole-cell patch-clamp technique in the current-clamp mode to stimulate the OHC at the base. The photometric response and the voltage response were monitored with a photodetector and patch-clamp amplifier, respectively. The photometric response was used to measure the regional changes in the membrane potential in response to maintained (dc) and sinusoidal (ac) current stimuli applied at the base of the cell. We used a neutral density filter to lower the excitation light intensity and reduce phototoxicity. A sensitive detector and lock-in amplifier were used to measure the small ac VSD signal. This permitted measurements of the ac photometric response below the noise floor of the static fluorescence. The amplitude and phase components of the photometric response were recorded for stimuli up to 800 Hz. VSD data at 400–800 Hz show the presence of a small phase delay between the stimulus voltage at the base of the cell and the local membrane potential measured along the lateral wall. Results are consistent with the hypothesis that OHCs exhibit inhomogeneous membrane potentials that vary with position in analogy with the voltage in nerve axons.

1. Introduction

Excitable cells have functional diversity because their voltage-dependent channels differ in ionic selectivity, modes of regulation and pharmacological properties (Hille 1992). Within a single cell there are also differences in channel distribution along the plasma membrane, and mammalian neurons have a physiological polarity critical to their function. For example, a high density of sodium channels exists at the nodes of Ranvier and differences in the surface densities of channels between somata and neuronal processes have been reported (Llinas and Sugimori 1980a, 1980b). More recently, the discovery of potassium channel density gradients in the dendrites of pyramidal neurons has intensified the study of such functional

E-mail: E-mail: brownell@bcm.tmc.edu.
[4]Present address: Department of Otorhinolaryngology, Faculty of Medicine Kyushu University, Fukuoka 812-8582, Japan.

inhomogeneities (Johnston *et al* 2000). Neither conventional microelectrode recordings nor patch-clamp recordings can assess regional variations in membrane voltage. However, employment of optical recording techniques using a fluorescent voltage-sensitive dye (VSD) enables measurement of spatiotemporal changes in the transmembrane voltage (Grinvald *et al* 1988, Cohen and Salzberg 1978).

There are two types of hair cells in the mammalian cochlea. Inner hair cells (IHCs) are the sensory cells that excite the primary afferent fibres. Outer hair cells (OHCs) are cylindrically shaped sensory cells and have a unique motile property (Brownell *et al* 1985, Dallos 1992). Changes in transmembrane potential evoke the OHC somatic motile response (Santos-Sacchi and Dilger 1988). Basilar membrane movement, evoked by a transmitted sound vibration, initiates the OHC receptor potential (Russell *et al* 1986) that drives somatic motility, refining basilar membrane movement in a feed-forward manner (Patuzzi and Robertson 1988). OHC electromotility contributes to the exquisite sensitivity and the fine frequency tuning of the cochlea (Brownell 1990, 2006, Brownell *et al* 2001, Snyder *et al* 2003, Oghalai 2004).

Previous reports have shown an uneven distribution of ionic channels in OHCs (Housley *et al* 1992, Nakagawa *et al* 1994, Santos-Sacchi *et al* 1997). Mechano-electrical transduction (MET) channels are located at the tips of stereocilia, which are inserted into the cuticular plate of the apical portion of the OHC (Hudspeth 1982). Both efferent and afferent fibres make synapses at the basal pole of OHCs where voltage-dependent channels (Roberts *et al* 1990) and ACh receptors are specifically located (Housley *et al* 1992). The lateral wall membrane is responsible for OHC electromotility, but it lacks voltage-dependent ion channels (Santos-Sacchi *et al* 1997). In addition to the heterogeneous distribution of ion channels in the plasma membrane, OHCs have a unique intracellular membrane bound organelle, the bilaminate, subsurface cisternae (SSC), that runs in close proximity to the lateral wall plasma membrane. It has been suggested previously that this structure might introduce regional differences in the timing and magnitude of local membrane potentials (Halter *et al* 1997). The unique polarized ultrastructure of the OHC and the heterogeneous distribution of membrane conductances led us to hypothesize that the OHC transmembrane voltage might express regional variations, particularly for stimulus frequencies above ~500 Hz.

To test this hypothesis we developed and applied methods to measure the regional OHC transmembrane potentials, using VSD photometrics, in response to command currents injected at the base of the cell. The amplitude and phase of photometric responses were successfully recorded for stimulus frequencies up to 800 Hz. Results showed the presence of small, but statistically significant, phase delays in the voltage response with position along the lateral wall.

2. Materials and methods

2.1. Solutions

The external solution contained 150 mM NaCl, 5 mM KCl, 2 mM $CaCl_2$, 1 mM $MgCl_2$, 10 mM HEPES and 10 mM glucose. The pH was adjusted to 7.4 with NaOH. The internal solution contained 150 mM KCl, 0.5 mM EGTA, 10 mM HEPES, 5 mM ATP-Na_2, 0.1 mM cAMP and 0.1 mM GTP-Na_2. The pH was adjusted to 7.3 with KOH.

2.2. Isolation of OHCs

The dissection procedure of the guinea pig OHCs was similar to that previously reported (Nakagawa *et al* 1990). Albino guinea pigs (weight 150–300 g) of either sex with good Preyer's reflexes were decapitated, and the temporal bones were removed. All procedures were performed in accordance with the Baylor College of Medicine institutional guidelines. The

bulla and bony shell of the cochlea were opened, and the organ of Corti with the attached modiolus kept in the external solution saturated with 100% O_2. The preparation was treated enzymatically with 0.5 mg ml^{-1} trypsin (Sigma, St. Louis, MO) and 0.5 mg ml^{-1} collagenase (Sigma, St. Louis, MO) at 31 °C for 3–5 min. The enzyme action was halted by washing the preparation with 0.1% bovine serum albumin (Sigma, St. Louis, MO). The organ of Corti was aspirated into a Pasteur pipette of 100–150 μm tip diameter, and the OHCs were isolated mechanically by gentle pipetting. Isolated OHCs were dispersed onto the 35 mm glass bottom poly-D-lysine coated Microwell dishes (MatTek Co, Ashland, MA).

2.3. Electrical recordings

Recording was performed in whole-cell configuration under either voltage clamp or current clamp. Glass pipettes were fabricated from borosilicate glass (G-1.5, Narishige, Tokyo, Japan) using a two-stage vertical puller (PP-83, Narishige, Tokyo, Japan). The resistance between the recording electrode filled with internal solution and the reference electrode was 3–6 MΩ. Data were recorded with an Axopatch 200B patch-clamp amplifier and a 12 bit acquisition board (Digidata 1200) controlled by pClamp 6.1 (Axon Instruments, Foster City, CA). The pipette seal (>1 GΩ) was always made below the nucleus. A whole-cell recording was established first in the voltage-clamp mode. Pipette capacitance, series resistance and cell capacitance were measured and compensated using the internal circuit of the amplifier. The series resistance was compensated by 70–90% during the voltage-clamp condition. For current-clamp experiments, the series resistance values obtained in voltage clamp were used for bridge balance compensation at a compensation ratio of 100%. Either current or voltage data were low-pass filtered at 10 kHz and sampled at 33 kHz. For FFT analysis, a spectrum analyser (Hewlett Packard 3567A) was used for on-line analysis. In this case, data were sampled at 6.4 kHz.

2.4. Voltage-sensitive dyes

A number of fast stryl-type VSDs were used, i.e., 3-(4-(2-(6-(dibutylamino)-2-naphthyl)-trans-ethenyl)pyridinium) propanesulfonate (di-4-ANEPPS), 1-(3-sulfonatopropyl)-4-[β[2-(di-n-octylamino)-6-naphthyl]vinyl]pyridinium betaine (di-8-ANEPPS), N-(4-sulfobutyl)-4-(4-(4-(dibutylamino) phenyl)hexatrienyl)pyridinium (RH-160), N-(4-sulfobutyl)-4-(6-(4-(dibutylamino)phenyl)butadienyl)pyridinium (RH-237), N-(3-triethylammoniumpropyl)-4-(4-(4-(diethylamino)phenyl) butadienyl)pyridinium (RH-414) and N-(4-sulfobutyl)-4-(4-(4-(dipentylamino)phenyl)butadienyl)pyridinium (RH-421), (Molecular Probes, Eugene, OR). Stock solutions (10 mM) were prepared by dissolving the dyes in DMSO, and kept in the dark at 4 °C. Fresh staining solutions were prepared immediately before the experiments by adding appropriate amounts of the gently warmed stock solution to the standard solutions (Bullen *et al* 1997). The dye concentration used for staining was between 30–100 μM, usually 50 μM. The OHCs were incubated with detergent-free staining solution for 10–20 min. After staining, OHCs were rinsed well with external solution. During the experiments, the chamber was constantly perfused with fresh external solution.

2.5. Optical recordings

Figure 1 is a schematic illustration of the experimental setup. The apparatus was built around an inverted microscope (Axiovert 135TV, Zeiss Inc., Thornwood, NY) mounted on a vibration isolation table (Micro-g, TMC, Peabody, MA). The objective lens used was a 63× oil immersion of N.A. 1.4 (Zeiss). The light from a xenon short arc lamp (75W, Osram, Munich, Germany; operated with a Model 1600 Power Supply, Opti Quip, Highland Mills, NY) was controlled by an electromechanical shutter (Uniblitz, Vincent Assoc. Rochester, NY) and was transmitted through fibre-optic cable (FSLE 34, Technical Video). The intensity of excitation light could be changed by a filter wheel equipped with absorptive neutral density filters (77384, Oriel Instruments, Stratford, CT). The exit aperture of a fibre-optic light source was positioned

at the field stop of the microscope such that the objective lens produced a 24 μm spot of excitation light on the cell (figure 2). The aperture of fibre optic was mounted on a three-dimensional hydraulic micromanipulator (MHW30, Narishige, Tokyo, Japan) so that the spot could be positioned to excite the VSD at various locations along the cell, without having to move the patch-clamped cell. The excitation filter was a 450–490 nm band-pass interference filter. The emission light was long-pass filtered above 520 nm. The fluorescence of the preparation collected by the objective lens was focused on a 1 mm × 1 mm single silicon photodiode (1336 K2G, Hamamatsu, Japan) located below the microscope. The emission light path could be manually switched between the eye pieces and the photodiode by removing 100% reflector in the microscope. During experiments, optical signals were recorded from three specific locations along the lateral wall of the OHC by moving the centre of the excitation light spot in steps of approximately 16.5 μm (see also figure 2). The photocurrent was passed to a custom-made current-to-voltage (*I–V*) converter with an initial feedback resistance of 3 GΩ. It contained three 1 GΩ resistors in series to reduce the parasitic capacity. With this layout, the converter acted as a low-pass filter with a corner frequency of 120 Hz. In later experiments, the feedback resistance was reduced down to 1 GΩ and the circuit layout was improved, resulting in a corner frequency of 1.2 kHz. The voltage output was sampled either at 3 kHz using a pClamp system (Axon Instrument, Foster City, CA), at 6.4 kHz with a spectrum analyser (Hewlett Packard 3567A), or by a digital signal processing lock-in amplifier SR830DSP, Stanford Research Systems, Stanford, CT; 1 s integration time, 24 dB/octave filter. The lock-in amplifier provides the amplitude and phase voltage signal. The phase of the photometric response at the base of the cell was set to zero and the phase at the other measurement locations was referenced to the base.

Care was taken to avoid phototoxicity associated with the formation of free radicals and membrane damage and cell depolarization (Grinvald *et al* 1988). We therefore continuously monitored the resting potential and rejected all data where the dc zero-current potential drifted more than 10 mV from the nominal −60 mV level at the beginning of each experiment. We also discarded all cells where the lock-in phase was not stable after 20 s (10 s lock-in integration and 10 s monitoring). Phototoxicity and rapid cell depolarization was problematic when using full strength illumination, and therefore a 10% neutral density filter was used in the excitation pathway.

2.6. Statistics

Paired Student *t*-tests were used to compare means; differences are reported as statistically significant if $p < 0.05$. Linear regression was performed using least-squares methods. All statistics were performed using Origin (Microcal Software, Northampton, MA).

2.7. Modelling

Experimental results were compared to the passive OHC model of Halter *et al* (1997) and to the piezoelectric model of Clifford *et al* (2006). Both of these models treat the OHC as a distributed voltage system, in analogy with the classical cable equation for axons. Regional differences in the membrane potential magnitude and phase arise in these models due to the presence of a relatively high axial resistance. The axial resistance is associated with restricting the axial current to flow in the model along the extracisternal space between the lateral membrane and the SSC. At low frequencies, the high axial resistance causes the magnitude of the voltage to decay with distance according to the space constant and introduces a frequency-dependent phase shift along the length. The phase φ(rad) of the plasma membrane potential relative to the voltage at the base of the cell can be interpreted as a time delay δ between the base and the measurement site (using $\delta = \varphi/\omega$, where ω is frequency in rad s^{-1}). Further, for cable equations, the time delay measured between two points separated by distance λ can be

used to estimate a phase velocity υ of a dispersive travelling wave using $\upsilon = \lambda/\delta$. It is this phase shift and associated phase velocity that is relevant to interpretation of the present data.

3. Results

3.1. Evaluation of different voltage-sensitive dyes

There are several types of fluorescent VSDs with different dynamics. Because the natural stimulus to the guinea pig OHC has a bandwidth of up to 40 kHz, we selected VSDs with fast response properties. Conditions for an appropriate dye are specific staining of the plasma membrane in the OHC, minimal phototoxicity, large static fluorescence (F), and a high voltage-sensitivity ($\Delta F/F$) (Grinvald *et al* 1988). Consistent with previous results (Oghalai *et al* 1998, 1999, 2000), di-8-ANEPPS specifically stained the plasma membrane of the OHC without visible uptake into the cells for at least an hour (see figure 2), whereas di-4-ANEPPS reached intracellular structures within 10 min. Also, the static fluorescence, F, and the voltage-dependent change of fluorescence, $\Delta F/F$, for RH-160, RH-237, RH-414, and RH-421 were significantly lower than that found for di-8-ANEPPS. In general, the magnitude of $\Delta F/F$ in the aminonaphthylethenylpyridinium (ANEP) dyes is considered to be smaller than that of the RH dyes (Fluhler *et al* 1985). However, in the OHC, the opposite was found to be the case. The average ± standard error (SE) of $\Delta F/F$ per 100 mV for di-8-ANEPPS was 2.6 ± 1.0% (n = 5), while that for the RH dyes was 0.42 ± 0.03% (n = 12). Therefore, di-8-ANEPPS, which has a time constant of about 10 μs (Grinvald *et al* 1988), was chosen as the VSD for all further experiments. It is fast enough for the present experiments where our highest stimulation frequency was 800 Hz.

3.2. Effects of di-8-ANEPPS staining on OHC ionic currents

To assess potential side effects of di-8-ANEPPS on the OHC, the resting potential and the current–voltage (I–V) relationships were observed before and after VSD staining. After establishing a whole-cell configuration, ionic currents of the OHC were recorded in the voltage-clamp mode. Both outward and inward currents were measured during depolarizing and hyperpolarizing voltage steps. The resting potential was then measured after switching to the current-clamp mode, and 100 μM di-8-ANEPPS was externally applied to the OHC for 20 min by Y-tube (Murase *et al* 1989). After ensuring good staining of the OHC plasma membrane by observation of the fluorescence, the cells were rinsed well and the chamber was constantly perfused with fresh external solution to wash out the excess dye and DMSO. The resting potential was checked and the membrane currents evoked by the voltage steps were recorded. The resting potentials pre- and post-staining were −69.5 ± 0.95 mV and −68.8 ± 0.88 mV (mean ± SEM; n = 8), respectively. There was no significant difference between these values (p = 0.33). Additionally, no changes in the I–V characteristics were observed (figure 3), indicating that di-8-ANEPPS staining does not affect OHC ionic currents. This is consistent with our previous findings (Oghalai *et al* 2000).

3.3. Photometric responses during injection of constant and sinusoidal currents

The voltage response measured by di-8-ANEPPS was compared to that recorded by the patch-clamp amplifier to examine the linearity and frequency characteristics. In our initial experiments, constant current steps were applied to the basal end of the OHC through the patch pipette using the current-clamp mode, while the whole-cell voltage response was monitored. The I–V converter of the photodiode was used at high gain, i.e., using a 3 GΩ feedback resistance. The excitation light spot was positioned on the base of the cell and the photometric response from this region was monitored. The optical signal was plotted as the change in fluorescence divided by the static fluorescence ($\Delta F/F$). Figure 4 compares a representative voltage and a photometric response to dc current step stimulation. Because of the low-pass filtering response of the photodiode I–V converter at high gain, the transient response of the

fluorescence at stimulus onset was somewhat lower than that of the patch-clamp amplifier. However, the relationship between the voltage amplitude and the photometric response at the steady-state level of each dc step stimulus was linear. For a population of 5 cells the $\Delta F/F$ per 100 mV change was 2.58 ± 0.34% (mean ± SEM; $n = 6$). The mean and SE of r values were 0.99 and 0.0013, respectively. p-values were less than 0.001 in all 5 cells (see the fit for the cell shown in figure 4). These data indicate that the photometric response reliably follows the membrane potential.

For the next experiments, sinusoidal current (3 nA peak-to-peak) was injected into the basal end of the OHC through the patch pipette. We used the *I–V* converter at low gain, i.e. with 1 GΩ feedback resistance in order to increase the corner frequency. Figure 5 compares representative photometric responses measured at the base of the cell and voltage responses as measured by the patch pipette. At 30, 60 and 120 Hz, the amplitude and phase of the photometric response followed the voltage response reliably. Therefore, these data indicate that optical measurements employing the VSD di-8-ANEPPS can be used to study the OHC membrane potential during application of both dc and ac currents.

In order to optically measure amplitude and phase of the membrane potential during application of higher frequency sinusoidal current, a lock-in amplifier was used. This permitted measurements of the photometric response below the noise floor of the static fluorescence, allowing us to use lower intensity excitation light together with the low gain setting on the photodetector *I–V* converter. Amplitude and phase were locked-in within 10 s of excitation light exposure, and were then monitored for 10 s. Typically, we found that amplitude and phase were stable when OHCs were stimulated by sinusoidal current of up to 1 kHz. Figure 6 shows the frequency characteristics of the voltage response recorded by the patch-clamp amplifier, the photometric response measured at the base of the cell, and the noise floor of the fluorescence measurement system (as measured by the spectrum analyser). The photometric response closely followed the voltage response.

We limited our current stimulation to three distinct frequencies: 100, 400 and 800 Hz, and compared the phase of the photometric response between the basal region and two positions along the lateral wall, intermediate 1 and intermediate 2 (see figure 2). Significant phase differences between regions could not be detected at 100 Hz. However, there were significant phase differences between the base and the lateral wall at both 400 Hz and 800 Hz (table 1). This was more pronounced as the spot moved closer to the apex, as seen by the lower p-value with these measures.

3.4. Modelling results

The OHC cable models exhibit cable properties including differences in the phase of the voltage at various locations in the cell (Halter *et al* 1997, Clifford *et al* 2006). The phase of the voltage predicted is sensitive to the location, dimensions, structure and biophysical properties of the cell. As a point of comparison, we considered an OHC from the apical turn of the guinea pig cochlea with a 9.6 μm diameter, 180 nm extracisternal gap for axial current flow, 0.04 S m^{-2} lateral wall plasma membrane conductance, 1.8 μF cm^{-2} membrane capacitance and 1.2 S-m m^{-2} intracellular conductivity. OHC cable models of this cell predict a 7.3°. phase delay at 400 Hz, and a 14° phase delay at 800 Hz, over a distance of 30 μm. Reducing the distance between recording sites to 15 μm cuts the phase delay in half (at these low frequencies). Adding piezoelectricity of 2.8 mC m^{-2} to the plasma membrane further increased the phase lag by a factor of approximately 1.7. In the active piezoelectric case, a 50 Hz pipette stimulus at the base evoked an isotonic displacement of 7.5 nm pA^{-1} and an isometric force of 5.8 pN pA^{-1}. The phase delays correspond to phase velocities of 2.9 m s^{-1} in the passive cable case and 1.6 m s^{-1} in the piezoelectric case. Cutting the axial resistance in half by doubling the size of the extracisternal space reduced the phase delay by a factor of 2 and doubled the corresponding

phase velocities. The range of delay times predicted by the models is consistent with the present experimental observations and thus lends support to the OHC cable hypothesis.

4. Discussion

Our results validate the use of di-8-ANEPPS to measure the transmembrane potential in the isolated OHC. This VSD provides both good linearity and frequency characteristics, consistent with results seen in other cell types (Bedlack *et al* 1994, Gross *et al* 1994, Bullen *et al* 1997, Zhang *et al* 1998, Bullen and Saggau 1999). However, the low $\Delta F/F$ makes data acquisition difficult secondary to the low signal-to-noise (S/N) ratio. Another problem that we had to face was the low-pass properties of the OHC when studied in the whole-cell mode. The resulting corner frequency is about 60 Hz (see figures 5 and 6) when the amplifier, pipette and cell membrane properties are considered. This causes the S/N ratio to decrease as the frequency increases. Increasing the gain of the photodiode $I–V$ converter increases the S/N ratio, but it lowers the frequency response. Increasing the intensity of the excitation light produces a larger emission, but also produces increased phototoxicity that leads to rapid cell death (Grinvald *et al* 1988). In addition, an excitation of di-8-ANEPPS inactivated non-linear capacitance by exposure of the intense light to the lateral membrane of the OHC with fibre-optic light guide (Santos-Sacchi and Zhao 2003). Since neither tradeoff was acceptable, we employed a lock-in amplifier to permit signal detection below the noise floor. We could decrease the intensity of light by inserting the neutral density filter in the path, resulting in a decrease in phototoxicity. We monitored the resting membrane potential and the phase fluctuation to check the cell's condition between each measurement. A decrease in capacitance would affect the membrane time constant and change the phase. After lowering the light intensity, this effect was not routinely found.

Photometric amplitude measurements could not be accurately compared between cell regions. Even though the excitation spot size remained constant, either the membrane area within the spot varied or staining could vary. An example of the first can be seen in figure 2, where there is an additional membrane visible on the basal end of the cell (likely from disrupted synaptic endings). This additional membrane would not undergo a change in membrane potential during OHC patch clamping. While both types of artefacts could result in variations of the magnitude of $\Delta F/F$ between regions, they would not affect phase measurements. Since the time constant of electromotility and di-8-ANEPPS is about 10 μs (Gale and Ashmore 1997,Grinvald *et al* 1988), there should be no effect of electromotility on the phase response, only the magnitude. Thus, we only analysed the phase data from our VSD experiments within a single OHC. The use of a ratiometric measurement technique may be a way to provide absolute membrane potential measurements in future experiments (Zhang *et al* 1998,Bullen and Saggau 1999).

It is typically assumed that the OHC plasma membrane is isopotential during physiological conditions and during whole-cell patch-clamp recordings. Present data are consistent with this description for low-frequency stimuli (e.g. <400 Hz) but show deviations at higher frequencies most relevant to the physiological range of hearing sensitivity. In particular, we observed statistically significant phase delays in the voltage acting across the lateral wall plasma membrane relative to the stimulus voltage at the base of the cell. The measured phase delays were inconsistent with the notion of 'space-clamp'. Rather, results are consistent with predictions of distributed-voltage cable models of the OHC (Halter *et al* 1997, Clifford *et al* 2006). The phase delay arises in these models due to a high intracellular axial resistance to current flow. The high resistance is described as due to the presence of the thin annular extracisternal space and restriction of current to flow along this space. Although it is clear that the SSC lines the plasma membrane lateral wall in OHCs, direct anatomical evidence that the axial current is completely restricted to the extracisternal space remains elusive. Present results provide electrical evidence consistent with this hypothesis.

If this hypothesis is true, there are two major physiological implications. First, current entering the transduction channels at the apical end of the cell will be divided between a relatively high axial resistance and the electromotile lateral membrane. The relatively high axial resistance will direct charge to the lateral wall and thereby increase the charge driven motile response. This would be expected to render the cell more sensitive to transduction current versus whole-cell voltage. Second, the cable-like properties render the electrical properties measured at low frequencies (e.g. whole-cell RC time constant) irrelevant at higher frequencies. These distributed cable properties may explain how OHCs overcome their passive whole-cell capacitance and maintain robust electromotile responses at high auditory frequencies.

Acknowledgments

The authors would like to thank Raphael RM, PhD, Bullen A, PhD Eatock RA, PhD and Ms Cindy Shope for their contribution to this study. This study was supported by grants from the Deafness Research Foundation and the National Institutes of Health (DC006671) to JSO and the National Institutes of Health (DC00354, DC02775 and DC04928) to WEB and RDR from NIDCD.

References

Bedlack RSJ, Wei M, Fox SH, Gross E, Loew LM. Distinct electric potentials in soma and neurite membranes. Neuron 1994;13:1187–93. [PubMed: 7946355]

Brownell WE. Outer hair cell electromotility and otoacoustic emissions. Ear Hear 1990;11:82–92. [PubMed: 2187727]

Brownell, WE. The piezoelectric outer hair cell. In: Eatock, RA., editor. Vertebrate Hair Cells. New York: Springer; 2006. p. 313-47.

Brownell WE, Bader CR, Bertrand D, de Ribaupierre Y. Evoked mechanical responses of isolated cochlear hair cells. Science 1985;227:194–6. [PubMed: 3966153]

Brownell WE, Spector AA, Raphael RM, Popel AS. Micro- and nanomechanics of the cochlear outer hair cell. Annu Rev Biomed Eng 2001;3:169–94. [PubMed: 11447061]

Bullen A, Patel SS, Saggau P. High-speed, random-access fluorescence microscopy: I. High-resolution optical recording with voltage-sensitive dyes and ion indicators. Biophys J 1997;73:477–91. [PubMed: 9199810]

Bullen A, Saggau P. High-speed, random-access fluorescence microscopy: II. Fast quantitative measurements with voltage-sensitive dyes. Biophys J 1999;76:2272–87. [PubMed: 10096922]

Clifford, S.; Brownell, WE.; Rabbitt, RD. Electro-mechanical waves in isolated outer hair cells. In: Nuttall, AL., et al., editors. Auditory Mechanisms: Processes and Models. Singapore: World Scientific; 2006. p. 146-54.

Cohen LB, Salzberg BM. Optical methods for monitoring neuron activity. Annu Rev Neurosci 1978;1:171–82. [PubMed: 386900]

Dallos P. The active cochlea. J Neurosci 1992;12:4575–85. [PubMed: 1464757]

Dieler R, Shehata-Dieler WE, Brownell WE. Concomitant salicylate-induced alterations of outer hair cell subsurface cisternae and electromotility. J Neurocytol 1991;20:637–53. [PubMed: 1940979]

Fluhler E, Burnham VG, Loew LM. Spectra, membrane binding, and potentiometric responses of new charge shift probes. Biochemistry 1985;24:5749–55. [PubMed: 4084490]

Gale JE, Ashmore JF. An intrinsic frequency limit to the cochlear amplifier. Nature 1997;389:63–6. [PubMed: 9288966]

Grinvald A, Frostig RD, Lieke E, Hildesheim R. Optical imaging of neuronal activity. Physiol Rev 1988;68:1285–366. [PubMed: 3054949]

Gross E, Bedlack RSJ, Loew LM. Dual-wavelength ratiometric fluorescence measurement of the membrane dipole potential. Biophys J 1994;67:208–16. [PubMed: 7918989]

Halter JA, Kruger RP, Yium MJ, Brownell WE. The influence of the subsurface cisterna on the electrical properties of the outer hair cell. Neuroreport 1997;8:2517–21. [PubMed: 9261819]

Hille, B. Ionic Channels of Excitable Membranes. Sunderland: Sinauer; 1992.

Housley GD, Ashmore JF. Direct measurement of the action of acetylcholine on isolated outer hair cells of the guinea pig cochlea. Proc R Soc B 1991;244:161–7.

Housley GD, Ashmore JF. Ionic currents of outer hair cells isolated from the guinea pig cochlea. J Physiol 1992;448:73–98. [PubMed: 1593487]

Housley GD, Greenwood D, Ashmore JF. Localization of cholinergic and purinergic receptors on outer hair cells isolated from the guinea-pig cochlea. Proc R Soc B 1992;249:265–73.

Hudspeth AJ. Extracellular current flow and the site of transduction by vertebrate hair cells. J Neurosci 1982;2:1–10. [PubMed: 6275046]

Johnston D, Hoffman DA, Magee JC, Poolos NP, Watanabe S, Colbert CM, Migliore M. Dendritic potassium channels in hippocampal pyramidal neurons. J Physiol 2000;525:75–81. [PubMed: 10811726]

Llinas R, Sugimori M. Electrophysiological properties of in vitro Purkinje cell somata in mammalian cerebellar slices. J Physiol 1980a;305:171–95. [PubMed: 7441552]

Llinas R, Sugimori M. Electrophysiological properties of in vitro Purkinje cell dendrites in mammalian cerebellar slices. J Physiol 1980b;305:197–213. [PubMed: 7441553]

Murase K, Ryu PD, Randic M. Excitatory and inhibitory amino acids and peptide-induced responses in acutely isolated rat spinal dorsal horn neurons. Neurosci Lett 1989;103:56–63. [PubMed: 2476693]

Nakagawa T, Akaike N, Kimitsuki T, Komune S, Arima T. ATP-induced current in isolated outer hair cells of guinea pig cochlea. J Neurophysiol 1990;63:1068–74. [PubMed: 2358862]

Nakagawa T, Kakehata S, Yamamoto T, Akaike N, Komune S, Uemura T. Ionic properties of IK, n in outer hair cells of guinea pig cochlea. Brain Res 1994;661:293–7. [PubMed: 7834381]

Oghalai JS. The cochlear amplifier: augmentation of the traveling wave within the inner ear. Curr Opin Otolaryngol Head Neck Surg 2004;12:431–8. [PubMed: 15377957]

Oghalai JS, Patel AA, Nakagawa T, Brownell WE. Fluorescence-imaged microdeformation of the outer hair cell lateral wall. J Neurosci 1998;18:48–58. [PubMed: 9412485]

Oghalai JS, Tran TD, Raphael RM, Nakagawa T, Brownell WE. Transverse and lateral mobility in outer hair cell lateral wall membranes. Heart Res 1999;135:19–28.

Oghalai JS, Zhao HB, Kutz JW, Brownell WE. Voltage-and tension-dependent lipid mobility in the outer hair cell plasma membrane. Science 2000;287:658–61. [PubMed: 10650000]

Patuzzi R, Robertson D. Tuning in the mammalian cochlea. Physiol Rev 1988;68:1009–82. [PubMed: 3054945]

Rabbitt RD, Ayliffe HE, Christensen D, Pamarthy K, Durney C, Clifford S, Brownell WE. Evidence of piezoelectric resonance in isolated outer hair cells. Biophys J 2005;88:2257–65. [PubMed: 15613632]

Roberts WM, Jacobs RA, Hudspeth AJ. Co–localization of ion channels involved in frequency selectivity and synaptic transmission at presynaptic active zones of hair cells. J Neurosci 1990;10:3664–84. [PubMed: 1700083]

Russell IJ, Cody AR, Richardson GP. The responses of inner and outer hair cells in the basal turn of the guinea-pig cochlea and in the mouse cochlea grown in vitro. Heart Res 1986;22:199–216.

Santos-Sacchi J, Dilger JP. Whole cell currents and mechanical responses of isolated outer hair cells. Heart Res 1988;35:143–50.

Santos-Sacchi J, Huang GJ, Wu M. Mapping the distribution of outer hair cell voltage-dependent conductances by electrical amputation. Biophys J 1997;73:1424–9. [PubMed: 9284309]

Santos-Sacchi J, Zhao H-B. Excitation of fluorescent dyes inactivates the outer hair cell integral membrane motor protein prestin and betray its lateral mobility. Pflugers Arch Eur J Physiol 2003;446:617–22. [PubMed: 12783229]

Snyder, KV.; Sachs, F.; Brownell, WE. The outer hair cell: A mechanoelectrical and electromechanical sensor/actuator. In: Barth, FG.; Humphrey, JAC.; Secomb, TW., editors. Sensors and Sensing in Biology and Engineering. Berlin: Springer; 2003. p. 71-95.

Zhang J, Davidson RM, Wei M, Loew LM. Membrane electric properties by combined patch clamp and fluorescence ratio imaging in single neurons. Biophys J 1998;74:48–53. [PubMed: 9449308]

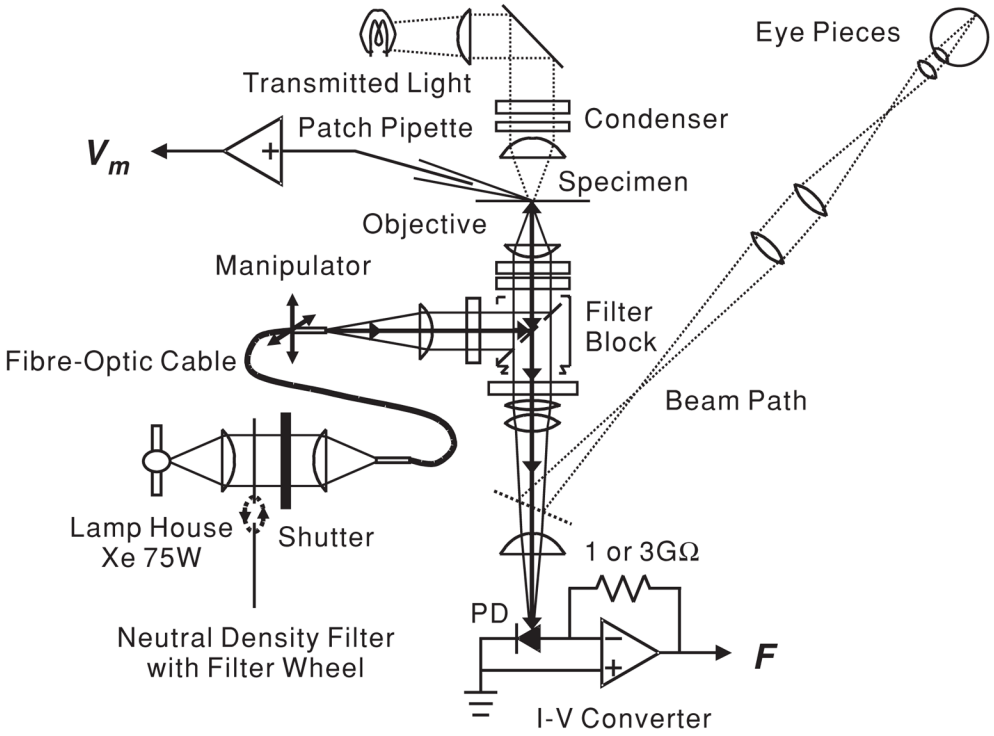

Figure 1.

Schematic diagram of the experimental set-up. The solid line represents the light path during VSD recordings. The position of the fibre-optic cable along the optical axis determines the spot size of the illumination spot on the OHC; its position in the plane perpendicular to the optical axis controls the location of the spot. The resistor across the operational amplifier in the *I–V* converter sets the feedback resistance, either 1 or 3 GΩ.

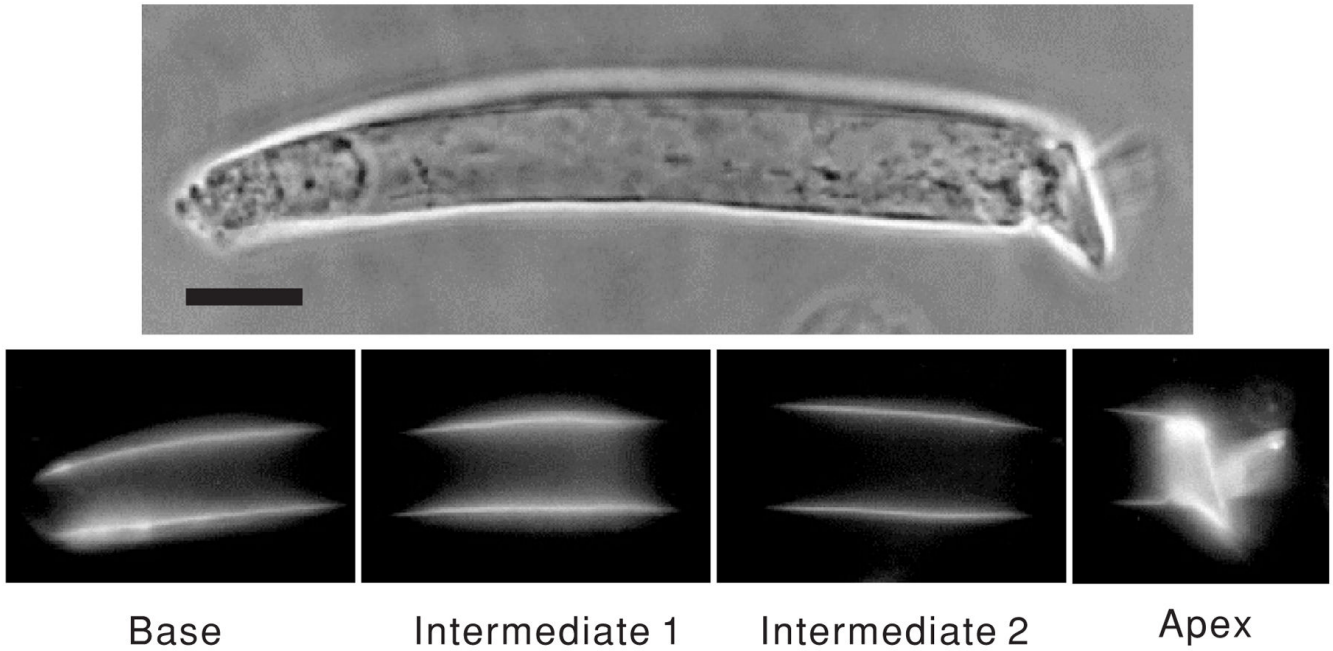

Figure 2.
OHCs stained with di-8-ANEPPS and images of an optically partitioned cell. From left to right, the excitation light was positioned in four distinct locations: base, intermediate 1, intermediate 2 and apex. Spot diameter was 24 μm. The centre of each location was separated by a distance of 16.5 μm. Horizontal bar indicated 10 μm.

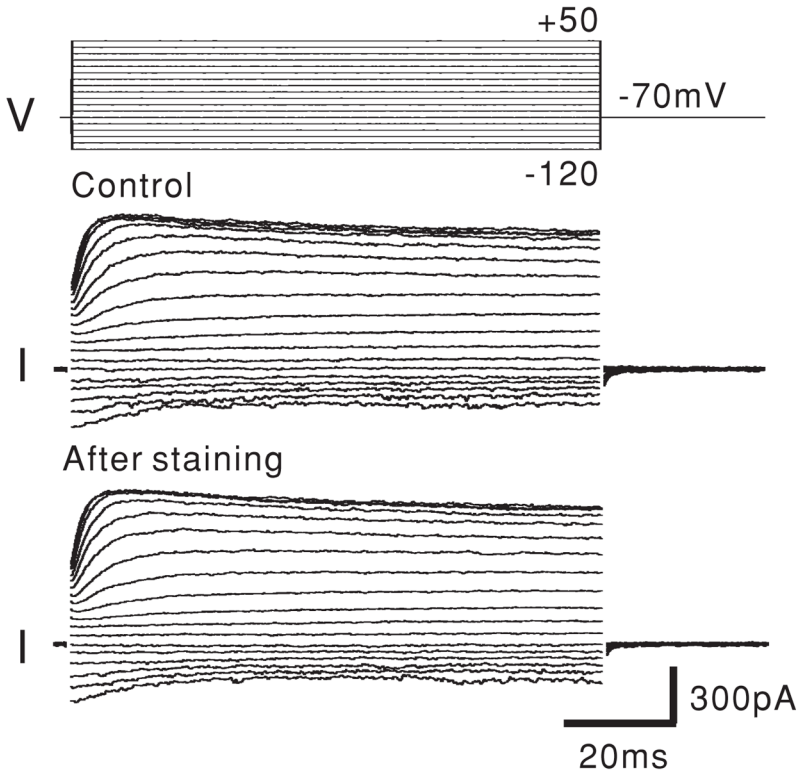

Figure 3.
The membrane currents of an OHC before and after di-8-ANEPPS staining show no effect from the VSD. This data were recorded in the voltage-clamp mode with a holding potential of −70 mV.

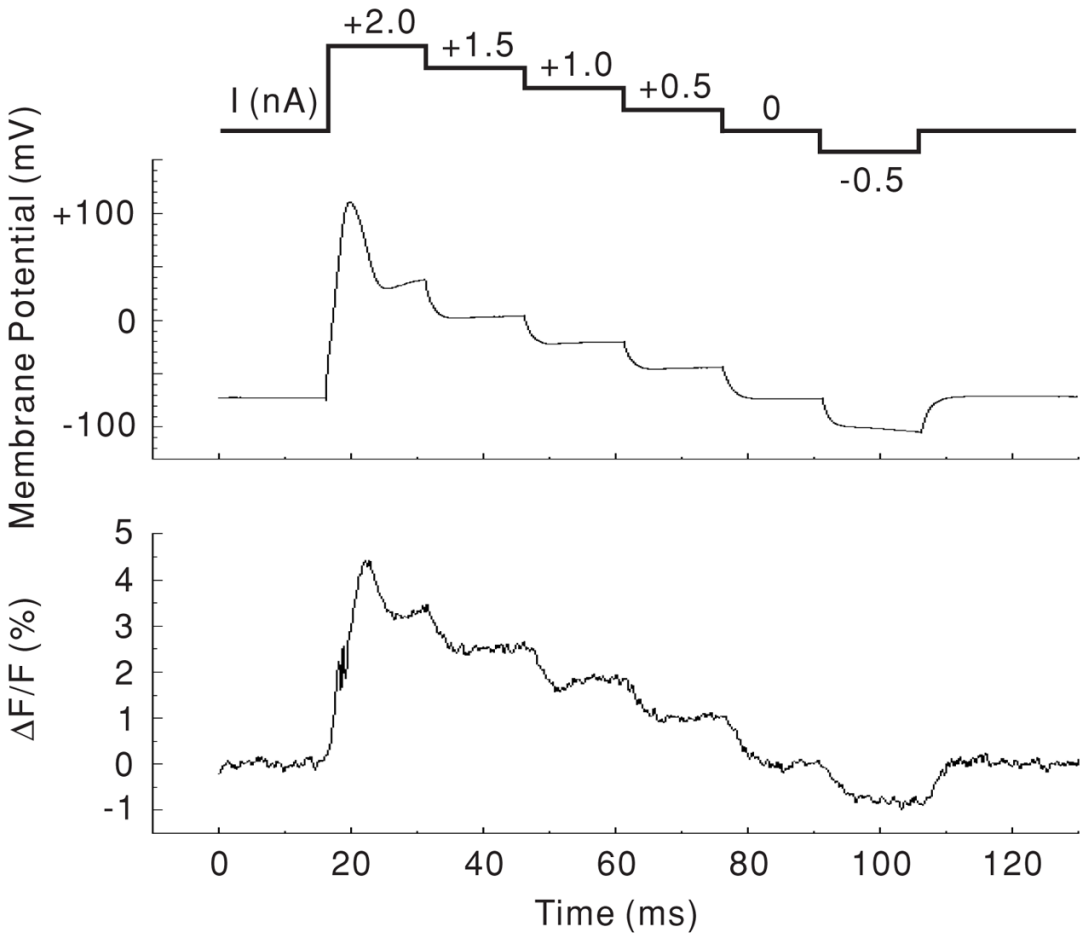

Figure 4.

DC response to step current injection. Both the membrane potential (as seen by the patch-clamp amplifier) and the photometric response (*ΔF*/*F*) were measured from the base of the OHC. The upper trace shows the stimulation protocol. Each trace is the average of four measurements. The data from this cell are fitted by *ΔF*/*F*;= 2.37 + 0.032 × MP (membrane potential) with an *r* value of 0.993 ($p < 0.001$).

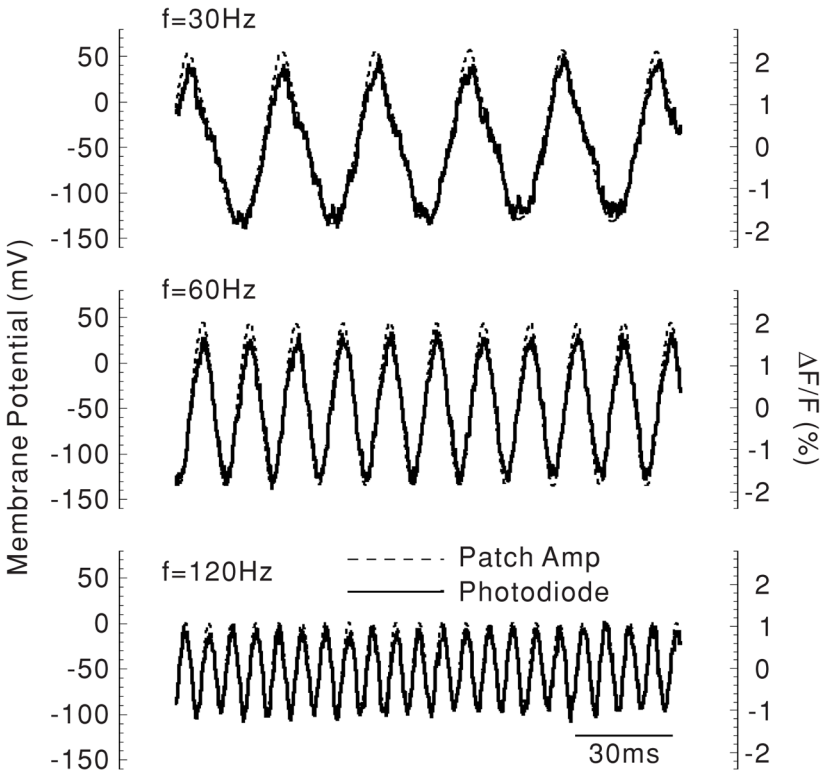

Figure 5.
AC response to sinusoidal current injection. Again, both the membrane potential and the photometric responses were measured from the base of the OHC. Each trace is the average of four measurements.

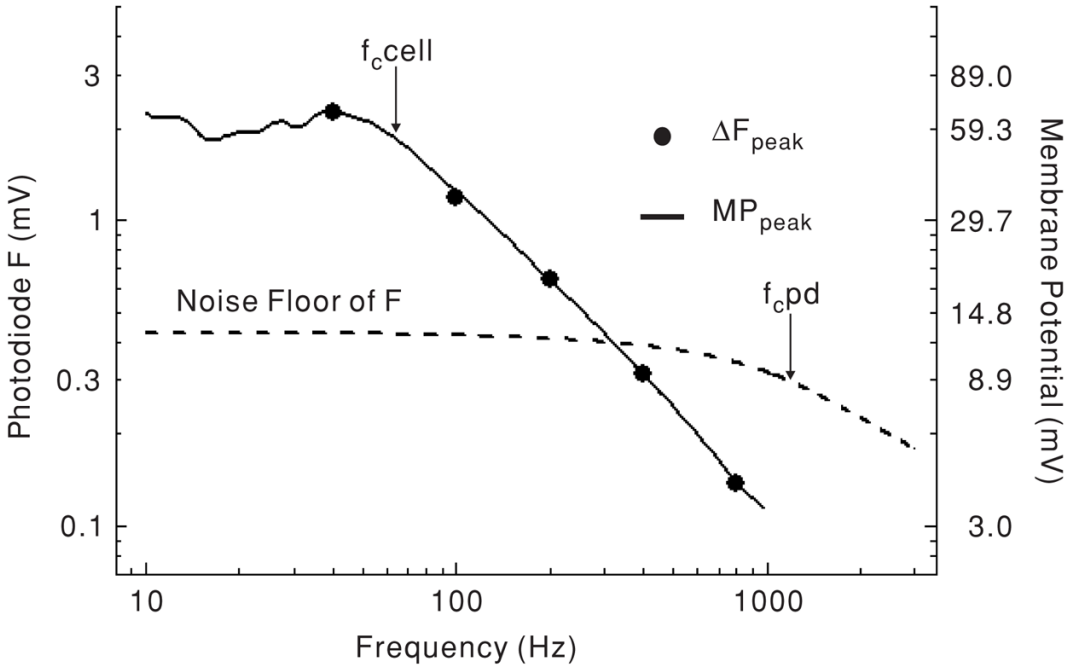

Figure 6.

Representative frequency responses of the membrane potential, the noise floor of the static fluorescence (*F*), and the photometric response at the base of the cell (*ΔF*). In this case, *ΔF* was plotted as a voltage (instead of a ratio) in order to compare it to the noise floor voltage. Note that *ΔF* could be recorded below the noise floor because the lock-in amplifier was used. All measurements are peak-to-peak values. Arrows show corner frequencies for the cell membrane potential (F_c cell) and the *I–V* converter of photodetector (f_c PD). Sine wave current injection (3 nA peak-to-peak) was used for stimulation.

Table 1

Phase shift of the photometric response. The OHC was stimulated at the base by a 3 nA peak-to-peak sinusoidal current injection of various frequencies under current clamp. The phase at the intermediate 1 and intermediate 2 segments was compared to the phase at the base using the paired Student's *t*-test.

	Phase shift from the base (°)		
Stimulus frequency (Hz)	**Intermediate 1**	**Intermediate 2**	***N***
100	4.2 ± 2.8, 0.19	10.7 ± 6.0, 0.15	6
400	−6.6 ± 2.4, 0.074	−11.5 ± 3.3, 0.041	4
800	−4.3 ± 1.2, 0.025	−6.9 ± 1.5, 0.011	5

The values in the second and third columns are mean ± SE, *p*-value.